

Interpretable Latent Variables in Deep State Space Models

Haoxuan Wu and David S. Matteson and Martin T. Wells
Department of Statistics and Data Science, Cornell University

Abstract

We introduce a new version of deep state-space models (DSSMs) that combines a recurrent neural network with a state-space framework to forecast time series data. The model estimates the observed series as functions of latent variables that evolve non-linearly through time. Due to the complexity and non-linearity inherent in DSSMs, previous works on DSSMs typically produced latent variables that are very difficult to interpret. Our paper focus on producing interpretable latent parameters with two key modifications. First, we simplify the predictive decoder by restricting the response variables to be a linear transformation of the latent variables plus some noise. Second, we utilize shrinkage priors on the latent variables to reduce redundancy and improve robustness. These changes make the latent variables much easier to understand and allow us to interpret the resulting latent variables as random effects in a linear mixed model. We show through two public benchmark datasets the resulting model improves forecasting performances.

1 Introduction

Time series forecasting has been an important area of research for long periods of time. This field has a wide range of inter-disciplinary applications such as forecasting economic variables [Siami-Namini and Namin, 2018], supply chain demands [De Gooijer and Hyndman, 2006] and demographic data [Montgomery et al., 2015]. With the advancements in technology and ever-looming presence of big data, the importance of producing accurate and interpretable forecasts for large, noisy datasets is higher than ever before. In this paper,

we propose a new approach for time series forecasting that produces both accurate predictions and interpretable latent variables.

A wide variety of methods have previously been utilized for time series forecasting. State-space models (SSMs) such as ARIMAs and dynamic linear models have been commonly used for this task [Hyndman and Khandakar, 2008, Aoki, 2013, Hyndman et al., 2002]. State-space models track the observed data as functions of latent variables that typically evolve linearly over time. SSMs produce interpretable forecasting results and have shown to be every effective at forecasting low-dimensional time-series data [Durbin and Koopman, 2012]. However, they tend to struggle in high dimensional settings, be inefficient with large datasets and are prone to high error propagation for long-term forecasting [Daum, 2005]. As a result, machine learning based methods such recurrent neural networks (RNN) have been frequently used as alternatives [Oancea and Ciucu, 2014, Connor et al., 1994]. RNNs, with the incorporation of long short term memory units [Hochreiter and Schmidhuber, 1997] or gated recurrent units [Chung et al., 2014], have shown to effective at forecasting high dimensional time series. However, a RNN by itself tends to be not enough to learn more intricate patterns in large datasets.

Deep state-space models (DSSMs) incorporate recurrent neural networks into a state-space framework to provide non-linear mappings of latent variables [Gedon et al., 2021]. In comparison to SSMs, DSSMs provide additionally flexibility in the estimation of the latent variables while maintaining the same general structure. By utilizing recurrent neural networks to learn global patterns across many series, DSSMs have proven to be effective at forecasting large datasets [Rangapuram et al., 2018]. Previous works have shown DSSMs to have comparable performance with other commonly used models such as DeepAR [Salinas et al., 2020], and Seasonal Autoregressive Integrated Moving Average with exogenous factors (SARIMAX).

At high level, existing machine learning methods are model-agnostic methods or innately interpretable models. The goal of model-agnostic methods is to explain predictions by a black-box approach. Alternatively, directly interpretable models such as generalized linear models (GLMs) [McCullagh and Nelder, 2019] are widely and successfully applied. Despite their effectiveness, one weakness of DSSMs is the lack of interpretability for the latent variables. For many of the existing work [Fraccaro et al., 2016, Chung et al., 2015, Krishnan et al., 2017], the observed data is assumed to follow a certain probability distribution whose sufficient statistics are calculated by a non-linear, black-box transformation of the latent variables. This transformation is typically parameterized through by a neural network. As a result, it becomes very difficult to explain the relationship between the observed and the latent variables. In this paper, we propose a new version of DSSM that produces interpretable latent variables while improving the forecasting performances. The details of our model will be shown in Section 3. We highlight two key contributions as follows.

First, our model restricts the mean of the observed variables to be a linear function of the latent variables. By restricting the decoder to be a simpler transformation, the relationship between the observed and the latent variables become much easier to understand. With a normal likelihood for the observed variables, our set-up allows the latent variables to be interpreted as random effects in a (generalized) linear mixed model with an exotic variance component [McCulloch and Searle, 2004].

Second, we incorporate shrinkage priors into the latent space to reduce redundancy and further enhance interpretability. Shrinkage priors have previous shown to be effective in SSMs [Cadonna et al., 2020, Kowal et al., 2019] and in other deep machine learning models [Bhadra et al., 2020, Louizos et al., 2017, Ghosh and Doshi-Velez, 2017]. We incorporate regularized horseshoe prior [Pironen and Vehtari, 2017, Ghosh et al., 2018] for the latent variables in order to induce more shrinkage toward zero. The resulting increased sparsity makes latent variables easier to understand and interpret. As we will show through two real-world benchmark datasets, shrinkage priors lead to more robustness and better forecasting performances. To the best of our knowledge, no previous work has used shrinkage priors directly on the latent variables in a DSSM setting.

2 Related Work

Variational autoencoder, introduced by Kingma and Welling [2013], produced an efficient method to es-

timate latent variables that are representative of the observed variables using variational inference. Since then, many works has been done expanding the structure and the application of the framework [Bayer and Osendorfer, 2014, Xue et al., 2020, Krishnan et al., 2017, Karl et al., 2016]. Chung et al. [2015] introduced variational recurrent neural network which utilizes high level latent variables to learn structure in sequential data. Fraccaro et al. [2016] extended the framework by incorporating a backward recurrent neural network to learn information from future observed variables. Krishnan et al. [2015] developed Deep Kalman Filter which utilized a non-linear autoregressive structure in the estimation of the latent variables. However, in most of above models, the observed variables are modeled as a non-linear transformation of the latent variables parameterized by neural networks. This set-up makes it very difficult to interpret the meaning of the latent variables.

One potential issue in the variational autoencoder framework is that no information is learned in the latent variables. To induce learning of global structure in the latent variables, three key areas of improvements have been made in recent works. First, simplifying the decoder in the generative model have shown to lead to more information stored in the latent [Gulrajani et al., 2016]. For example, Chen et al. [2016] utilized noisy version of historical data in the generative process to induce robustness in the latent variables. By utilizing a simpler decoder, more information has to be stored in the latent to achieve similar performances. Second, the loss can be modified to induce more structures in the latent variables. Bowman et al. [2015] utilized KL-annealing to induce lower weight on the KL-divergence term in the loss function to allow for better learning in the training process. Goyal et al. [2017] added auxiliary variables into the network to ensure the observed can be reconstructed through the latent variables. Third, Rezende and Mohamed [2015] introduced the idea of normalizing flow which induces a more flexible, scalable class of posterior distributions. Kingma et al. [2016] and Louizos and Welling [2017] expanded on this idea for better approximate posteriors. Most of these works have been focused on the area of NLP or image recognition. We adopt some of ideas for time series analysis and take it one step further. In addition to ensuring the latent variables contain useful information, our model also ensures these variables are interpretable.

Within the class of deep state-space models, arguably the most interpretable version is the model introduced by Rangapuram et al. [2018]. In their model, the recurrent neural network estimated the coefficients of a Gaussian state-space model and Kalman Filtering was

used to update the latent variables. By utilizing the RNN only for modeling of the coefficients, the model avoided the need for variational inference. While this model maintained a state-space structure, the coefficients themselves may freely change over-time. This makes it difficult to understand the true underlying relationship between the observed and the latent variables. The other work in a DSSM context focused on interpretability is the model introduced by [Li et al., 2019]. The paper utilized automatic relevance determination network to select relevant covariates for each time-step. Unlike their work which focused on interpretability in covariate selection, our work focuses on interpretability in terms of latent variables.

3 Methodology

3.1 Cost Function

Suppose we have observed time series $\mathbf{y}_{1:T}$ with $\{y_t \in \mathbb{R}^M\}_{t=1}^T$ and a set of covariates $\mathbf{u}_{1:T}$ with $\{u_t \in \mathbb{R}^N\}_{t=1}^T$. For our version of the deep state-space model, we assume the observed variables are functions of latent variables $\mathbf{z}_{1:T}$ with $\{z_t \in \mathbb{R}^Q\}_{t=1}^T$. Suppose further the latent variables depend on a recurrent neural network with output variables $\mathbf{h}_{1:T}$, a set of global variables \mathbf{g} and a set of local variables $\boldsymbol{\lambda}_{1:T}$. We will detail each of these variables in Subsection 3.2. Let $\boldsymbol{\theta}$ denote all parameters associated with the DSSM such as weights for the neural networks. We can write the loss as follows:

$$\begin{aligned} L(\boldsymbol{\theta}; \mathbf{y}_{1:T}, \mathbf{u}_{1:T}) &= L(\boldsymbol{\theta}) \\ &\equiv \log \int p_{\boldsymbol{\theta}}(\mathbf{y}_{1:T}, \mathbf{z}_{1:T}, \mathbf{h}_{1:T}, \mathbf{g}, \boldsymbol{\lambda}_{1:T} | \mathbf{u}_{1:T}) \\ &\quad d\mathbf{z}_{1:T} d\mathbf{h}_{1:T} d\mathbf{g} d\boldsymbol{\lambda}_{1:T} \end{aligned} \quad (1)$$

Due to the complexity of the model, this integral is intractable. As a result, we will use an inference model to estimate an approximate posterior $q_{\boldsymbol{\phi}}(\mathbf{z}_{1:T}, \mathbf{h}_{1:T}, \mathbf{g}, \boldsymbol{\lambda}_{1:T} | \mathbf{y}_{1:T}, \mathbf{u}_{1:T})$ with a set of inference parameters $\boldsymbol{\phi}$. The inference model is utilized to approximate the true posterior $p_{\boldsymbol{\theta}}(\mathbf{z}_{1:T}, \mathbf{h}_{1:T}, \mathbf{g}, \boldsymbol{\lambda}_{1:T} | \mathbf{y}_{1:T}, \mathbf{u}_{1:T})$. Using Jensen's inequality, Equation 1 can be bounded by:

$$\begin{aligned} L(\boldsymbol{\theta}) &\geq E_{q_{\boldsymbol{\phi}}(\cdot)} \left[\log \frac{p_{\boldsymbol{\theta}}(\mathbf{y}_{1:T}, \mathbf{z}_{1:T}, \mathbf{h}_{1:T}, \mathbf{g}, \boldsymbol{\lambda}_{1:T} | \mathbf{u}_{1:T})}{q_{\boldsymbol{\phi}}(\mathbf{z}_{1:T}, \mathbf{h}_{1:T}, \mathbf{g}, \boldsymbol{\lambda}_{1:T} | \mathbf{y}_{1:T}, \mathbf{u}_{1:T})} \right] \\ &= E_{q_{\boldsymbol{\phi}}(\cdot)} \left[\log p_{\boldsymbol{\theta}}(\mathbf{y}_{1:T} | \mathbf{z}_{1:T}, \mathbf{h}_{1:T}, \mathbf{g}, \boldsymbol{\lambda}_{1:T}, \mathbf{u}_{1:T}) \right] \\ &\quad - \text{KL} \left(q_{\boldsymbol{\phi}}(\mathbf{z}_{1:T}, \mathbf{h}_{1:T}, \mathbf{g}, \boldsymbol{\lambda}_{1:T} | \mathbf{y}_{1:T}, \mathbf{u}_{1:T}) \parallel \right. \\ &\quad \left. p_{\boldsymbol{\theta}}(\mathbf{z}_{1:T}, \mathbf{h}_{1:T}, \mathbf{g}, \boldsymbol{\lambda}_{1:T} | \mathbf{y}_{1:T}, \mathbf{u}_{1:T}) \right) \end{aligned} \quad (2)$$

where $q_{\boldsymbol{\phi}}(\cdot) = q_{\boldsymbol{\phi}}(\mathbf{z}_{1:T}, \mathbf{h}_{1:T}, \mathbf{g}, \boldsymbol{\lambda}_{1:T} | \mathbf{y}_{1:T}, \mathbf{u}_{1:T})$. Equation 2 is also known as the Variational Evidence Lower Bound (ELBO). The first term is a reconstruction loss

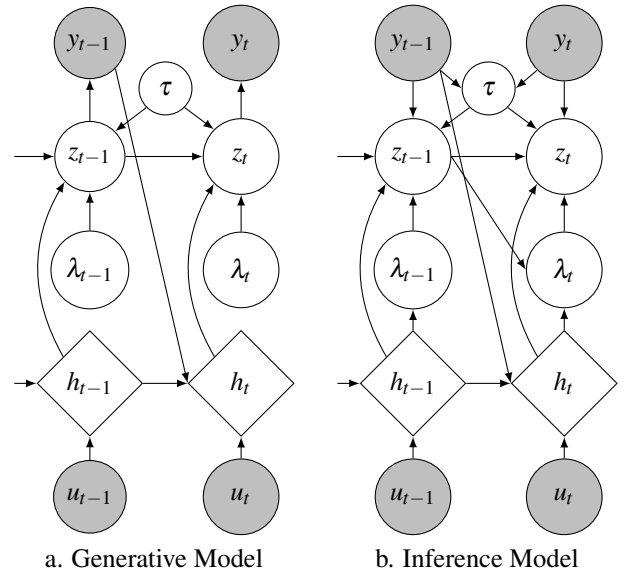


Figure 1: Details of the processes for the generative and inference portions of the DSSM model. Deterministic components are shown by diamonds; latent variables are shown by unshaded circles and the rest are shown by shaded circles.

composed of the expected log-likelihood. This term encourages the approximate posterior from the inference model to properly explain the observed variables. The second term is the KL-divergence between the prior and the approximate posterior. This term encourages the approximate posterior to be close to the prior. The resulting model can be decomposed into two parts: a generative model to estimate the joint distribution and an inference model to estimate the posterior for the latent variables.

To ensure the ELBO can be estimated effectively, we design the model (seen in Figure 1) to allow for closed-form estimation of the KL-divergence term. A closed form solution avoids sampling from $p_{\boldsymbol{\theta}}(\mathbf{z}_{1:T}, \mathbf{h}_{1:T}, \mathbf{g}, \boldsymbol{\lambda}_{1:T} | \mathbf{y}_{1:T}, \mathbf{u}_{1:T})$ during training and speeds up estimation of the loss. Our choices for the generative/inference portions of the model will be detailed in Subsections 3.2 and 3.3. A more detailed explanation for the variational inference steps are shown in the Appendix.

3.2 Generative Model

The generative portion of the model can be seen in Figure 1, Part a. The joint distribution can be factorized as

follows:

$$\begin{aligned} p_{\boldsymbol{\theta}}(\mathbf{y}_{1:T}, \mathbf{z}_{1:T}, \mathbf{h}_{1:T}, \mathbf{g}, \boldsymbol{\lambda}_{1:T} | \mathbf{u}_{1:T}) \\ = p_{\boldsymbol{\theta}}(\mathbf{g}) \prod_{t=1}^T p_{\boldsymbol{\theta}}(\mathbf{y}_t | \mathbf{z}_t) p_{\boldsymbol{\theta}}(\mathbf{z}_t | \mathbf{h}_t, \mathbf{z}_{t-1}, \boldsymbol{\lambda}_t, \mathbf{g}) \\ p_{\boldsymbol{\theta}}(\mathbf{h}_t | \mathbf{h}_{t-1}, \mathbf{y}_{t-1}, \mathbf{u}_t) p_{\boldsymbol{\theta}}(\boldsymbol{\lambda}_t) \end{aligned} \quad (3)$$

The generative model composed of estimating two global distributions and four time-specific distributions. The global part consists of estimating \mathbf{g} while the time-specific part consists of estimating $\boldsymbol{\lambda}_t$ and three conditional distributions. We will detail the choice and the reasoning for each of the distributions below, starting with $p_{\boldsymbol{\theta}}(\mathbf{y}_t | \mathbf{z}_t)$. Note the initial variables $(\mathbf{z}_0, \mathbf{y}_0, \mathbf{h}_0)$ are omitted from the equations for clarity; they are all initialized to be zero in implementation.

3.2.1 Generation of Latent Variables

To allow for more efficient posterior sampling [Ingraham and Marks, 2016], we write $p_{\boldsymbol{\theta}}(\mathbf{z}_t | \mathbf{h}_t, \mathbf{z}_{t-1}, \boldsymbol{\lambda}_t, \mathbf{g})$ in non-centered parameterization form as follows:

$$\mathbf{z}_t \sim \mathbf{z}_t^* + \boldsymbol{\tau}_t^* \boldsymbol{\lambda}_t. \quad (4)$$

The prior for \mathbf{z}_t can be decomposed into two parts: a normal prior given by \mathbf{z}_t^* and shrinkage components given by $\boldsymbol{\tau}_t^* \boldsymbol{\lambda}_t$. Note that $\boldsymbol{\tau}_t^*$ is a function of both \mathbf{g} and $\boldsymbol{\lambda}_t$, details will be shown in Equation 8.

Note that \mathbf{z}_t^* is a function of the output of the recurrent neural network from the current time-step and the latent variables from the previous time-step.

$$\mathbf{z}_t^* \sim N(\boldsymbol{\mu}_{\boldsymbol{\theta}, \mathbf{z}}(\mathbf{h}_t, \mathbf{z}_{t-1}), \boldsymbol{\Sigma}_{\boldsymbol{\theta}, \mathbf{z}}(\mathbf{h}_t, \mathbf{z}_{t-1})) \quad (5)$$

where the parameters $\boldsymbol{\mu}_{\boldsymbol{\theta}, \mathbf{z}}(\mathbf{h}_t, \mathbf{z}_{t-1}) = NN_{\boldsymbol{\theta}, 1}(\mathbf{h}_t, \mathbf{z}_{t-1})$ and $\boldsymbol{\Sigma}_{\boldsymbol{\theta}, \mathbf{z}}(\mathbf{h}_t, \mathbf{z}_{t-1}) = \text{SoftPlus}(NN_{\boldsymbol{\theta}, 2}(\mathbf{h}_t, \mathbf{z}_{t-1}))$ in which NN denote a feed-forward neural network. Note we use different numbered subscripts to denote that the feed-forward neural networks are different.

3.2.2 Generation of Shrinkage Variables

The shrinkage components $\boldsymbol{\tau}_t^*$ and $\boldsymbol{\lambda}_t$ are the regularized global and local components of the shrinkage prior placed on the latent variables. The purpose of these terms is to reduce redundancy and add additional robustness. We chose the regularized horseshoe prior [Pironen and Vehtari, 2017] because it has strong posterior contraction properties and has previously shown to be effective in a variational inference setting [Ghosh et al., 2018]. The regularized horseshoe prior is similar to the standard horseshoe [Carvalho et al., 2009] but with a bound on the upper tail. It falls under the class of global-local shrinkage priors with a global component to track overall shrinkage and local components

to track shrinkage at each time-step. This set-up allows for strong global shrinkage while still maintaining localized adaptivity. We will discuss our choice for the local components $\boldsymbol{\lambda}_t$ first followed by the global component.

Suppose there are Q latent variables estimated at each time-step, the regularized horseshoe models each of the variables $\boldsymbol{\lambda}_t = [\lambda_{t,1}, \dots, \lambda_{t,Q}]$ independently using a standard half-Cauchy distribution denoted by $C^+(0, 1)$. Since approximating the posterior directly from a half-Cauchy distribution can be difficult, we will use the decomposition to write the half-Cauchy as a combination of a Gamma and an inverse-Gamma distribution [Neville et al., 2014].

$$\begin{aligned} \lambda_{t,i}^2 &= \alpha_{t,i} \beta_{t,i} & \text{for } i = 1, \dots, Q \\ \alpha_{t,i} &\sim G(0.5, 1) & \beta_{t,i} \sim IG(0.5, 1) \end{aligned} \quad (6)$$

where $G(a, b)$ and $IG(a, b)$ is the Gamma and inverse-Gamma distribution with shape parameter a and scale parameter b .

The global component of the model consists of two variables: $\mathbf{g} = (\tau, c)$. τ estimates global amount of shrinkage across all time-steps and c controls the upper bound for the shrinkage components. Details for these components will be given in Equation 7 and 9. A similar decomposition can be used for $p_{\boldsymbol{\theta}}(\tau)$. In a regularized horseshoe prior, $\tau \sim C^+(0, \tau_0)$ where τ_0 is a hyperparameter.

$$\begin{aligned} \tau^2 &= \alpha_{\tau} \beta_{\tau} \\ \alpha_{\tau} &\sim G(0.5, \tau_0^2) & \beta_{\tau} \sim IG(0.5, 1). \end{aligned} \quad (7)$$

One potential issue of the half-Cauchy distribution is the fat tail which may lead to undesirable, large values for the latent variables. To bound the upper limit of the shrinkage prior, we write $\boldsymbol{\tau}_t^* = [\tau_{t,1}^*, \dots, \tau_{t,Q}^*]$ as follows:

$$\tau_{t,i}^{*2} = \frac{c^2 \tau^2}{c^2 + \tau^2 \lambda_{t,i}^2} \quad \text{for } i = 1, \dots, Q \quad (8)$$

where c is a weight decay variable for controlling the upper-bound. With this set-up, in time-steps when $\tau^2 \lambda_{t,i}^2 \gg c^2$, $\tau_{t,i}^{*2} \lambda_{t,i}^2 \rightarrow c^2$. In time-steps when $\tau^2 \lambda_{t,i}^2 \ll c^2$, $\tau_{t,i}^{*2} \lambda_{t,i}^2 \rightarrow \tau^2 \lambda_{t,i}^2$, which is the standard horseshoe. As a result, the regularized version maintains the strong posterior contraction of the horseshoe prior while avoiding arbitrarily high values for the latent variables. As recommended by Pironen and Vehtari [2017], we place an inverse gamma prior on c^2 with two hyperparameters c_0 and c_1 :

$$c^2 \sim IG(c_0, c_1) \quad (9)$$

3.2.3 Generation of Response / RNN Variables

As previous discussed in Section 1, we restrict $\{\mathbf{y}_t\}_{t=1}^T$ to be a linear transformation of the latent variables plus some noise component. Assuming \mathbf{y}_t follows normal distribution, $p_{\theta}(\mathbf{y}_t|\mathbf{z}_t)$ can be written as follows:

$$\mathbf{y}_t \sim N(\mathbf{A}_{\theta}\mathbf{z}_t, \boldsymbol{\sigma}_{\theta,\mathbf{y}}(\mathbf{z}_t)) \quad (10)$$

where $\boldsymbol{\sigma}_{\theta,\mathbf{y}}(\cdot) = \text{SoftPlus}(NN_{\theta,3}(\mathbf{z}_t))$ and \mathbf{A}_{θ} is a linear transformation. We adopt the SoftPlus transformation, previously seen in Li et al. [2019], to ensure that the standard deviation is non-negative. We allow the standard deviation to be a non-linear transformation of the latent variables to give additional flexibility for complex noises. Setting \mathbf{A}_{θ} as non-time-varying makes the relationship between the predicted response and the latent variables easier to understand. As we will discuss in Section 3.5, this set-up allows $\{\mathbf{z}_t\}$ to be interpreted as random effects in a linear mixed model.

The variables $\{\mathbf{h}_t\}$ are estimated in a deterministic manner via a recurrent neural network with gated recurrent units. Recurrent neural network unfolds along the temporal horizon, making it a natural choice for the time series modeling. We write the update equation as follows:

$$\mathbf{h}_t = \delta(\text{GRU}_{\theta}(\mathbf{h}_{t-1}, \mathbf{u}_t, \mathbf{y}_{t-1})) \quad (11)$$

where $\text{GRU}(\cdot)$ is gated recurrent unit update and $\delta(\cdot)$ is the delta-Dirac function.

3.3 Inference Model

The inference portion of the model can be seen in Figure 1, Part b. We approximate the true posterior with the following factorization:

$$q_{\phi}(\mathbf{z}_{1:T}, \mathbf{h}_{1:T}, \mathbf{g}, \boldsymbol{\lambda}_{1:T} | \mathbf{y}_{1:T}, \mathbf{u}_{1:T}) = q_{\phi}(\mathbf{g} | \mathbf{y}_{1:T}) \prod_{t=1}^T q_{\phi}(\mathbf{z}_t | \mathbf{z}_{t-1}, \mathbf{y}_t, \mathbf{h}_t, \mathbf{g}, \boldsymbol{\lambda}_t) q_{\phi}(\boldsymbol{\lambda}_t | \mathbf{z}_{t-1}, \mathbf{h}_t) p_{\theta}(\mathbf{h}_t | \mathbf{h}_{t-1}, \mathbf{y}_{t-1}, \mathbf{u}_t) \quad (12)$$

For the inference portion, we estimate the posterior for the global variables \mathbf{g} using all available observed variables. Two posterior distributions are calculated at each time-step: an estimation for posterior of \mathbf{z}_t and an estimation for the posterior of $\boldsymbol{\lambda}_t$. Since \mathbf{h}_t is deterministic, we use the same network as the generative portion. The key to the inference step is finding an appropriate family for the posterior of each variable to allow for estimation of intractable posterior seen in Equation 1. We will explain the choice and reasoning for each of the posteriors below, starting with $q_{\phi}(\mathbf{z}_t | \mathbf{z}_{t-1}, \mathbf{y}_t, \mathbf{h}_t, \boldsymbol{\tau}, c, \boldsymbol{\lambda}_t)$.

3.3.1 Inference of Latent Variables

Due to the non-centered parameterization for the generative model seen in Equation 4, we adopt a similar parameterization for the approximate posterior. Note we use tilde notation to indicate the posterior estimates for the variables from the inference network.

$$\begin{aligned} \tilde{\mathbf{z}}_t &\sim \tilde{\mathbf{z}}_t^* \tilde{\boldsymbol{\tau}}_t^* \tilde{\boldsymbol{\lambda}}_t \\ \tilde{\mathbf{z}}_t^* &\sim N(\boldsymbol{\mu}_{\phi,\tilde{\mathbf{z}}}(\tilde{\mathbf{z}}_{t-1}, \mathbf{y}_t, \mathbf{h}_t), \boldsymbol{\sigma}_{\phi,\tilde{\mathbf{z}}}(\tilde{\mathbf{z}}_{t-1}, \mathbf{y}_t, \mathbf{h}_t)) \end{aligned} \quad (13)$$

where $\boldsymbol{\mu}_{\phi,\tilde{\mathbf{z}}}(\tilde{\mathbf{z}}_{t-1}, \mathbf{y}_t, \mathbf{h}_t) = NN_{\phi,1}(\tilde{\mathbf{z}}_{t-1}, \mathbf{y}_t, \mathbf{h}_t)$, $(\tilde{\boldsymbol{\tau}}_t^*, \tilde{\boldsymbol{\lambda}}_t)$ denote the approximate posteriors for the shrinkage variables and $\boldsymbol{\sigma}_{\phi,\tilde{\mathbf{z}}}(\tilde{\mathbf{z}}_{t-1}, \mathbf{y}_t, \mathbf{h}_t) = \text{SoftPlus}(NN_{\phi,2}(\tilde{\mathbf{z}}_{t-1}, \mathbf{y}_t, \mathbf{h}_t))$. With this set-up, the posterior for the latent variables can be expressed as $\tilde{\mathbf{z}}_t \sim N(\boldsymbol{\mu}_{\phi,\tilde{\mathbf{z}}}(\tilde{\mathbf{z}}_{t-1}, \mathbf{y}_t, \mathbf{h}_t) \tilde{\boldsymbol{\tau}}_t^* \tilde{\boldsymbol{\lambda}}_t, \boldsymbol{\sigma}_{\phi,\tilde{\mathbf{z}}}(\tilde{\mathbf{z}}_{t-1}, \mathbf{y}_t, \mathbf{h}_t) \tilde{\boldsymbol{\tau}}_t^* \tilde{\boldsymbol{\lambda}}_t)$. This allows $\tilde{\mathbf{z}}_t$ to be viewed as a scale mixture of normals with scales $\tilde{\boldsymbol{\tau}}_t^* \tilde{\boldsymbol{\lambda}}_t$.

3.3.2 Inference of Shrinkage Variables

From Equation 6, we see that each of the $\tilde{\boldsymbol{\lambda}}_t = [\tilde{\lambda}_{t,1}, \dots, \tilde{\lambda}_{t,Q}]$ is modeled independently by a gamma and an inverse gamma distribution. We approximate each using a log-normal distribution. We choose log-normal distribution as it has a closed form KL-divergence with Gamma/Inverse-Gamma prior [Louizos and Welling, 2017] and allows for efficient sampling [Ghosh and Doshi-Velez, 2017]. The approximate posterior looks as follows:

$$\begin{aligned} \tilde{\lambda}_{t,i}^2 &= \tilde{\alpha}_{t,i} \tilde{\beta}_{t,i} && \text{for } i = 1, \dots, Q \\ \tilde{\alpha}_{t,i} &\sim LN(\boldsymbol{\mu}_{\phi,\alpha,t,i}(\mathbf{z}_{t-1}, \mathbf{h}_t), \boldsymbol{\sigma}_{\phi,\alpha,t,i}(\mathbf{z}_{t-1}, \mathbf{h}_t)) \\ \tilde{\beta}_{t,i} &\sim LN(\boldsymbol{\mu}_{\phi,\beta,t,i}(\mathbf{z}_{t-1}, \mathbf{h}_t), \boldsymbol{\sigma}_{\phi,\beta,t,i}(\mathbf{z}_{t-1}, \mathbf{h}_t)) \end{aligned} \quad (14)$$

where $LN(\cdot, \cdot)$ represents a log-normal distribution. The posterior parameters $(\boldsymbol{\mu}_{\phi,\alpha,t,i}(\mathbf{z}_{t-1}, \mathbf{h}_t), \boldsymbol{\sigma}_{\phi,\alpha,t,i}(\mathbf{z}_{t-1}, \mathbf{h}_t), \boldsymbol{\mu}_{\phi,\beta,t,i}(\mathbf{z}_{t-1}, \mathbf{h}_t), \boldsymbol{\sigma}_{\phi,\beta,t,i}(\mathbf{z}_{t-1}, \mathbf{h}_t))$ are each estimated through a feed-forward neural network.

The posterior for the global portion of the shrinkage prior $\mathbf{g} = (\boldsymbol{\tau}, c)$ are estimated conditional on the entirety of the observed data. We adopt two log-normal distributions for the approximate posterior of $\boldsymbol{\tau}$. An additional log-normal will be used as the posterior of c .

$$\begin{aligned} \tilde{\boldsymbol{\tau}} &= \tilde{\alpha}_{\boldsymbol{\tau}} \tilde{\beta}_{\boldsymbol{\tau}} \\ \tilde{c} &\sim LN(\boldsymbol{\mu}_{\phi,c}(\mathbf{y}_{1:T}), \boldsymbol{\sigma}_{\phi,c}(\mathbf{y}_{1:T})) \\ \tilde{\alpha}_{\boldsymbol{\tau}} &\sim LN(\boldsymbol{\mu}_{\phi,\alpha,\boldsymbol{\tau}}(\mathbf{y}_{1:T}), \boldsymbol{\sigma}_{\phi,\alpha,\boldsymbol{\tau}}(\mathbf{y}_{1:T})) \\ \tilde{\beta}_{\boldsymbol{\tau}} &\sim LN(\boldsymbol{\mu}_{\phi,\beta,\boldsymbol{\tau}}(\mathbf{y}_{1:T}), \boldsymbol{\sigma}_{\phi,\beta,\boldsymbol{\tau}}(\mathbf{y}_{1:T})) \end{aligned} \quad (15)$$

where once again $(\mu_{\phi,c}(\mathbf{y}_{1:T}), \sigma_{\phi,c}(\mathbf{y}_{1:T}), \mu_{\phi,\alpha,\tau}(\mathbf{y}_{1:T}), \sigma_{\phi,\alpha,\tau}(\mathbf{y}_{1:T}), \mu_{\phi,\beta,\tau}(\mathbf{y}_{1:T}), \sigma_{\phi,\beta,\tau}(\mathbf{y}_{1:T}))$ are all feed-forward neural networks. These neural networks takes average of all observed variables as inputs to allow for varying length sequences. Conditional on $(\tilde{\tau}, \tilde{c}, \tilde{\lambda}_t)$, $\tilde{\tau}_t^*$ can be estimated in a similar fashion to Equation 8:

$$\tilde{\tau}_t^{*2} = \frac{\tilde{c}^2 \tilde{\tau}^2}{\tilde{c}^2 + \tilde{\tau}^2 \tilde{\lambda}_t^2}. \quad (16)$$

3.4 Variational Inference / Forecasting Procedures

Estimating the expectation term in Equation 2 remains a difficult task. To reduce the variance of the estimator, we utilize Stochastic Gradient Variational Bayes [Kingma and Welling, 2013, Rezende et al., 2014] and the reparameterization trick. At each time step, we sample $q_{\phi}(\tau|\mathbf{y}_{1:T})$, $q_{\phi}(c|\mathbf{y}_{1:T})$ and $q_{\phi}(\lambda_t|\mathbf{z}_{t-1}, \mathbf{h}_t)$ from the log-normal posterior distributions. However, instead of directly sampling from $q_{\phi}(\mathbf{z}_t|\mathbf{z}_{t-1}, \mathbf{y}_t, \mathbf{h}_t, \tau, c, \lambda_t)$, we sample from auxiliary random variables $\tilde{\mathbf{e}}_t \sim N(\mathbf{0}, \mathbf{I})$ where \mathbf{I} is the identity matrix. We then obtain samples of the posterior through a transformation the auxiliary variables as follows: $\tilde{\mathbf{z}}_t = \tilde{\mathbf{e}}_t \odot \tilde{\sigma}_{\mathbf{z},t} + \tilde{\mu}_{\mathbf{z},t}$ where \odot is element-wise product, $\tilde{\mu}_{\mathbf{z},t} = \mu_{\phi,\tilde{\mathbf{z}}}(\tilde{\mathbf{z}}_{t-1}, \mathbf{y}_t, \mathbf{h}_t) \tilde{\tau}_t^* \tilde{\lambda}_t$ and $\tilde{\sigma}_{\mathbf{z},t} = \sigma_{\phi,\tilde{\mathbf{z}}}(\tilde{\mathbf{z}}_{t-1}, \mathbf{y}_t, \mathbf{h}_t) \tilde{\tau}_t^* \tilde{\lambda}_t$. By utilizing auxiliary random variables, we separate the source of randomness from the posterior parameters in which the gradients are required. This, in turn, reduces the variance of the gradient estimators.

During testing time, Monte Carlo samples will be utilized to generate forecasts from the model. Suppose the goal is to forecast $p(\mathbf{y}_{(T+1):(T+p)}|\mathbf{y}_{1:T}, \mathbf{u}_{1:(T+p)})$ with p denoting the forecasting horizon. First, we sample global variables from their approximate posterior $q_{\phi}(c, \tau|\mathbf{y}_{1:T})$ using the sequence of known observed values. The sampled values will be used in all time-steps in the forecasting horizon.

Next, for each time-step from 1 to T , we iteratively estimate all time-dependent variables using both the generative and the inference portions of the model. The latent variables will be sampled from the posterior distribution $q_{\phi}(\mathbf{z}_t|\mathbf{z}_{t-1}, \mathbf{y}_t, \mathbf{h}_t, \tau, c, \lambda_t)$ until the last known time-step. For each time-step t in the forecasting horizon from $T+1$ to $T+p$, we iteratively update the model to obtain updates as follows:

$$\begin{aligned} \tilde{\mathbf{y}}_{T+t} &\sim N(\mathbf{A}_{\theta} \mathbf{z}_{T+t}, \sigma_{\theta, \mathbf{y}}(\mathbf{z}_t)) \\ \mathbf{z}_{T+t} &= \mathbf{z}_{T+t}^* \tilde{\mathbf{v}}_{T+t}^* \tilde{\lambda}_{T+t} \\ \mathbf{z}_{T+t}^* &\sim N(\mu_{\theta, \mathbf{z}}(\mathbf{h}_{T+t}, \mathbf{z}_{T+t-1}), \sigma_{\theta, \mathbf{z}}(\mathbf{h}_{T+t}, \mathbf{z}_{T+t-1})) \\ \mathbf{h}_{T+t} &= \delta(\text{GRU}_{\theta}(\mathbf{h}_{T+t-1}, \mathbf{u}_{T+t}, \tilde{\mathbf{y}}_{T+t-1})) \end{aligned}$$

where $\tilde{\mathbf{y}}_{T+t-1}$ is the sampled response from the previous time-step. $\tilde{\lambda}_{T+t}$ is sampled using Equation 14 and τ_{T+t}^* is calculated using Equation 8.

One note to highlight is that we sample the variables associated with the shrinkage prior from the inference model and the latent variables from the generative model. This is due to the fact that in the inference model, estimation of $\tilde{\mathbf{z}}_t^*$ requires \mathbf{y}_t which makes it infeasible during testing time. In contrast, we specifically designed the estimation for the approximate posterior of the shrinkage variables to not rely on \mathbf{y}_t . This choice allows the shrinkage variables to be sampled from their approximate posteriors which provide more information.

3.5 Latent Variables Interpretability

As previously mentioned, directly interpretable models such as generalized linear models (GLMs) [McCullagh and Nelder, 2019] have been widely and successfully applied. Equation 10 shows the relationship between the response and the latent variables. From the set-up, it's clear that $\{\mathbf{A}_{\theta} \mathbf{z}_t\}$ is the linear predictor component of the normal likelihood. By utilizing a linear layer rather than a deep neural network in the generative framework, the model makes the relationship between the response and the latent variables much easier to understand, therefore enhancing the interpretability of the latent variables. Furthermore, shrinkage priors are utilized to borrow strength across the variables [Fourdrinier et al., 2018, Seto et al., 2021] in order to reduce redundancy in the latent variables. In particular, from Equations 4 - 11 one can see that the latent variables can be interpreted as random effects in a linear mixed model with an exotic variance component.

4 Real Data Analysis

We utilize two datasets for our analysis: *electricity* and *traffic*. Both datasets are publicly available under the UCI machine learning directory. *Electricity* contains electricity usage of 370 customers, aggregated at an hourly level. *Traffic* contains occupancy rate between 0 and 1 of 440 car lanes on the San Francisco freeways, also aggregated at an hourly level. These 2 datasets represent challenging forecasting problems as they are large datasets containing long-term trends and daily/weekly seasonal fluctuations. These datasets have also been evaluated in previous work [Rangapuram et al., 2018, Salinas et al., 2020], making them good benchmarks for comparisons.

Throughout the simulations, we will refer the model introduced in Section 3 as deep state-space model with shrinkage (DSSM-SH). We will compare against

Table 1: Forecasting comparison across 4 models in terms of normalised deviation and normalised root mean squared error for the *electricity* dataset.

	ARIMA	DeepAR	DSSM-NS	DSSM-SH
ND	0.342	0.079	0.071	0.066
RMSE	0.892	0.661	0.516	0.502

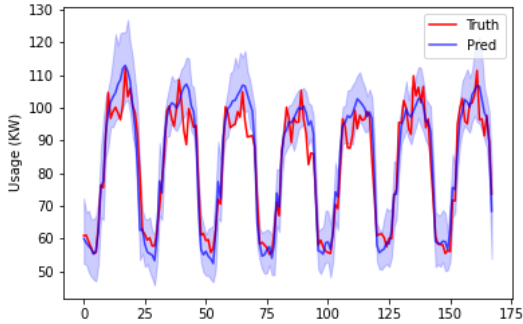


Figure 2: 1 week rolling forecast of a series from the *electricity* dataset over the testing horizon. x-axis indicate number of hours ahead in the forecasting horizon. Red line indicate true usage value, blue line indicate predicted value from DSSM-SH with 95% posterior credible bands in light blue.

2 competitors: ARIMA and DeepAR [Salinas et al., 2020]. ARIMA will act as a state-space model benchmark for these datasets; we utilize the `auto.arima` function R package `forecast` for automatic selection of orders. DeepAR utilizes a recurrent neural network for prediction. DeepAR has less components on top of the RNN compared to DSSM-SH, making it a good machine learning benchmark for comparison. We will also compare our model against a variant of DSSM-SH but with the shrinkage components removed denoted by DSSM-NS. Without shrinkage components, the model is very similar to a standard DSSM.

For each of the models, we generate $n = 50$ number of Monte Carlo samples for each time-step in the forecasting horizon. Two metrics will be used to evaluate the accuracy of predicted samples for each model: normalised deviation (ND) and normalised root mean squared error (RMSE). Suppose in the testing set, we wish to forecast N series each with forecasting length p . The metrics are defined as follows:

$$\text{ND} = \frac{\sum_{n=1}^N \sum_{t=1}^p |y_{t,i} - \tilde{y}_{t,i}|}{\sum_{n=1}^N \sum_{t=1}^p |y_{t,i}|}$$

$$\text{RMSE} = \frac{\sqrt{\frac{1}{Np} \sum_{n=1}^N \sum_{t=1}^p (y_{t,i} - \tilde{y}_{t,i})^2}}{\frac{1}{Np} \sum_{n=1}^N \sum_{t=1}^p |y_{t,i}|}$$

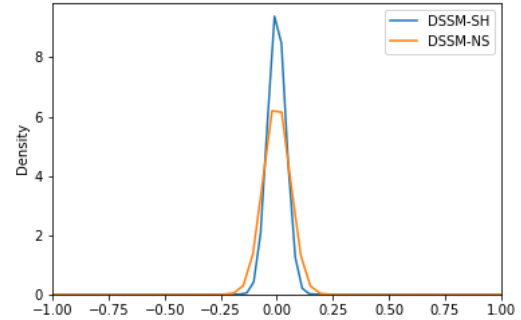


Figure 3: Kernel density estimation of distribution of latent variables in the testing set for DSSM-SH and DSSM-NS.

where $y_{t,i}$ is the true observed value for i th series in the testing set at forecast time-step t and $\tilde{y}_{t,i}$ is the median of the predicted samples from the model. These metrics present good evaluation metrics as they measure average deviation between the true values and the predicted values.

4.1 Electricity Dataset

Electricity dataset contains hourly usage across many month. We utilize data from January 1, 2014 to September 1, 2014 for training/validation and data from September 1, 2014 to September 8, 2014 for testing. We evaluate the forecasting performances of the models over a forecast horizon of 48 hours with a learning period of 144 hours. Following [Salinas et al., 2020], each input series is standardized using a series dependent scale factor. This standardization process allows for efficient handling of drastically change scales inherent in the dataset. The models are implemented via Pytorch using NVIDIA Tesla K80 GPU. All details concerning the set-up of the models and hyperparameter turning are given in the Appendix.

The results for the models can be seen in Table 1. As seen in the table, DSSM-SH outperformed all competitors in terms both of normalised deviation and normalised root mean squared error. This indicates that DSSM-SH does not sacrifice forecasting accuracy in return for interpretable latent variables. Despite simplifying the expected value of observed variables to be

Table 2: Forecasting comparison across 4 models in terms of normalised deviation and normalised root mean squared error for the *traffic* dataset.

	ARIMA	DeepAR	DSSM-NS	DSSM-SH
ND	0.372	0.178	0.134	0.123
RMSE	1.324	0.433	0.391	0.373

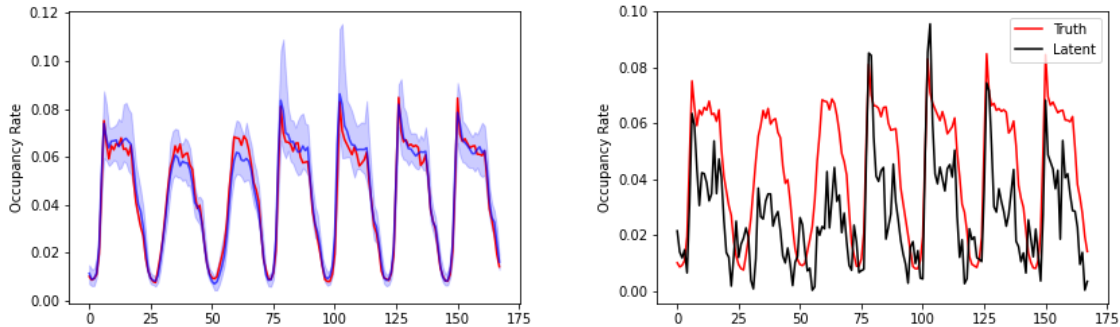


Figure 4: Left plot shows 1 week rolling forecast from DSSM-SH of a series from the *traffic* dataset over test horizon of 1 week. x-axis indicate number of hours ahead in the forecasting horizon. Right plot shows the same series with the absolute value of the average latent variable values at each time-step plotted in black.

a linear function of the latent variables, DSSM-SH still manages to improve the forecasting results. Comparing DSSM-SH and DSSM-NS, we can see that adding shrinkage priors slightly improves the forecasting results. As seen, shrinkage priors are shown to induce more robustness against over-fitting the training data.

Figure 2 illustrates forecasting result from DSSM-SH over 1 week test horizon for a series in *electricity*. We can see that the data contains daily fluctuations and shifts in volatility. State-space models like to ARIMA tend to struggle to capture the long-term dependencies as reflected by the high ND metric. DeepAR, while performing much better than ARIMA, tends to miss some more intricate patterns due to just using a recurrent neural network. DSSM-SH, as shown in the figure, is able to capture the long term trends and seasonal patterns inherent in the data.

Figure 3 compares the distribution of $\{z_t\}_{t=1}^T$ across the entire testing set for DSSM-SH and DSSM-NS. As seen in the figure, DSSM-SH has a much higher density near 0, indicating the result of incorporating shrinkage priors. The use of structured horseshoe priors in DSSM-SH push more latent variables closer toward zero in comparison to DSSM-NS. This leads to increased shrinkage and decreased redundancy in the latent variables, highlighting the benefits of shrinkage priors.

4.2 Traffic Dataset

The *traffic* dataset contains 15 month of occupancy rate for San Francisco freeways. We utilize data before June 15, 2008 for training/validation and data from June 15, 2008 to June 22, 2008 for testing. Similar to electricity, we utilize a forecasting horizon of 48 hours with a learning period of 144 hours. The result comparing the various models can be seen in Table 2.

As seen in the results, DSSM-SH performs the best in terms of both normalised deviation and normalised root mean squared error. ARIMA struggles with long term forecasting as reflected by the high RMSE. The gap between DSSM-SH and DeepAR widens in comparison to the results from *electricity*. This further highlights the benefits of using a deep state-space framework in comparison to just using a recurrent neural network. Comparing DSSM-NS with DSSM-SH, we can see that the deep state-space model with shrinkage prior performed slightly better. This supports the benefit of having shrinkage priors in terms of adding robustness to the model.

Left plot of Figure 4 illustrates an example of the resulting forecasting of DSSM-SH on a series from the *traffic* dataset. The plot is generated using a rolling forecast [Nicholson et al., 2017] with a window of 48 hours across the one week testing horizon. As seen in the results, DSSM-SH is able to capture the long-term patterns inherent in the data and make accurate prediction throughout the forecasting horizon. 50 samples

are generated at each forecasting step; the blue bands seen in the figure reflects 95th percentile and 5th percentile of the samples. In time-steps with high occupancy rate, we see that the band becomes wider, reflecting the fact that there exist more volatility in the underlying data. In time-steps where the occupancy rate starts to decrease to a lower level, the band becomes much narrower, reflecting a higher confidence from DSSM-SH about the underlying value. This shows that DSSM-SH is able to capture well the true underlying mean and volatility throughout the forecasting horizon.

Right plot of Figure 4 shows the absolute value of average latent variables values sampled at each time-step. Suppose there are B samples generated and Q latent variables sampled at forecasting time-step t , the value of the black-line at time-step t is calculated as $|\frac{1}{QB} \sum_{j=1}^B \sum_{i=1}^Q z_{t,i}^{(j)}|$. The notation $z_{t,i}^{(j)}$ indicates the value of the i th latent variable at time t for Monte Carlo sample j . We took the absolute value of the average to make the relationship easier to visualize. As seen in the figure, there exist a strong correlation between the magnitude of the response and the average value of the latent variables. High average latent values lead to higher predicted response values. This highlights the key benefit of simplifying the decoder to be a linear function. The relationship between the response and the latent variables become much clear to understand, leading to more interpretability for the latent variables.

5 Conclusion

In this paper, we introduced a deep state-space model (DSSM-SH) with the ability to produce interpretable latent variables. Our two key modifications to the DSSM framework are restricting the relationship between the response and the latent variables to be a linear function plus some noise component, and incorporating regularized horseshoe priors for the latent variables. As we have shown through two real world benchmark datasets, these modifications lead to more interpretable latent results and improved forecasting performances. Our model outperforms both ARIMA (a state-space model) and DeepAR (a RNN based model), showing the effectiveness of the DSSM framework in combining the two parts. In comparison to DSSM-NS, a deep state-space model without shrinkage, our model performs slightly better in forecasting metrics. This shows that add shrinkage priors reduce redundancy and improve robustness.

References

- Masanao Aoki. *State space modeling of time series*. Springer Science & Business Media, 2013.
- Justin Bayer and Christian Osendorfer. Learning stochastic recurrent networks. *arXiv preprint arXiv:1411.7610*, 2014.
- Anindya Bhadra, Jyotishka Datta, Yunfan Li, and Nicholas Polson. Horseshoe regularisation for machine learning in complex and deep models. *International Statistical Review*, 88(2):302–320, 2020.
- Samuel R Bowman, Luke Vilnis, Oriol Vinyals, Andrew M Dai, Rafal Jozefowicz, and Samy Bengio. Generating sentences from a continuous space. *arXiv preprint arXiv:1511.06349*, 2015.
- Annalisa Cadonna, Sylvia Frühwirth-Schnatter, and Peter Knaus. Triple the gamma—a unifying shrinkage prior for variance and variable selection in sparse state space and tvp models. *Econometrics*, 8(2):20, 2020.
- Carlos M Carvalho, Nicholas G Polson, and James G Scott. Handling sparsity via the horseshoe. In *Artificial Intelligence and Statistics*, pages 73–80. PMLR, 2009.
- Xi Chen, Diederik P Kingma, Tim Salimans, Yan Duan, Prafulla Dhariwal, John Schulman, Ilya Sutskever, and Pieter Abbeel. Variational lossy autoencoder. *arXiv preprint arXiv:1611.02731*, 2016.
- Junyoung Chung, Caglar Gulcehre, KyungHyun Cho, and Yoshua Bengio. Empirical evaluation of gated recurrent neural networks on sequence modeling. *arXiv preprint arXiv:1412.3555*, 2014.
- Junyoung Chung, Kyle Kastner, Laurent Dinh, Kratarth Goel, Aaron C Courville, and Yoshua Bengio. A recurrent latent variable model for sequential data. *Advances in neural information processing systems*, 28:2980–2988, 2015.
- Jerome T Connor, R Douglas Martin, and Les E Atlas. Recurrent neural networks and robust time series prediction. *IEEE transactions on neural networks*, 5(2):240–254, 1994.
- Fred Daum. Nonlinear filters: beyond the kalman filter. *IEEE Aerospace and Electronic Systems Magazine*, 20(8):57–69, 2005.
- Jan G De Gooijer and Rob J Hyndman. 25 years of time series forecasting. *International journal of forecasting*, 22(3):443–473, 2006.
- James Durbin and Siem Jan Koopman. *Time series analysis by state space methods*. Oxford university press, 2012.

- Dominique Fourdrinier, William E Strawderman, and Martin T Wells. *Shrinkage estimation*. Springer, 2018.
- Marco Fraccaro, Søren Kaae Sønderby, Ulrich Paquet, and Ole Winther. Sequential neural models with stochastic layers. *arXiv preprint arXiv:1605.07571*, 2016.
- Daniel Gedon, Niklas Wahlstrom, Thomas B. Schon, and Lennart Ljung. Deep state space models for nonlinear system identification. *IFAC-PapersOnLine*, 54:481–486, 2021.
- Soumya Ghosh and Finale Doshi-Velez. Model selection in bayesian neural networks via horseshoe priors. *arXiv preprint arXiv:1705.10388*, 2017.
- Soumya Ghosh, Jiayu Yao, and Finale Doshi-Velez. Structured variational learning of bayesian neural networks with horseshoe priors. In *International Conference on Machine Learning*, pages 1744–1753. PMLR, 2018.
- Anirudh Goyal, Alessandro Sordoni, Marc-Alexandre Côté, Nan Rosemary Ke, and Yoshua Bengio. Z-forcing: Training stochastic recurrent networks. In *NIPS*, 2017.
- Ishaan Gulrajani, Kundan Kumar, Faruk Ahmed, Adrien Ali Taiga, Francesco Visin, David Vazquez, and Aaron Courville. Pixelvae: A latent variable model for natural images. *arXiv preprint arXiv:1611.05013*, 2016.
- Sepp Hochreiter and Jürgen Schmidhuber. Long short-term memory. *Neural computation*, 9(8):1735–1780, 1997.
- Rob J Hyndman and Yeasmin Khandakar. Automatic time series forecasting: the forecast package for r. *Journal of statistical software*, 27(1):1–22, 2008.
- Rob J Hyndman, Anne B Koehler, Ralph D Snyder, and Simone Grose. A state space framework for automatic forecasting using exponential smoothing methods. *International Journal of forecasting*, 18(3):439–454, 2002.
- John B Ingraham and Debora S Marks. Bayesian sparsity for intractable distributions. *arXiv preprint arXiv:1602.03807*, 2016.
- Maximilian Karl, Maximilian Soelch, Justin Bayer, and Patrick Van der Smagt. Deep variational bayes filters: Unsupervised learning of state space models from raw data. *arXiv preprint arXiv:1605.06432*, 2016.
- Diederik P Kingma and Max Welling. Auto-encoding variational bayes. *arXiv preprint arXiv:1312.6114*, 2013.
- Durk P Kingma, Tim Salimans, Rafal Jozefowicz, Xi Chen, Ilya Sutskever, and Max Welling. Improved variational inference with inverse autoregressive flow. *Advances in neural information processing systems*, 29:4743–4751, 2016.
- Daniel R Kowal, David S Matteson, and David Ruppert. Dynamic shrinkage processes. *Journal of the Royal Statistical Society: Series B (Statistical Methodology)*, 81(4):781–804, 2019.
- Rahul Krishnan, Uri Shalit, and David Sontag. Structured inference networks for nonlinear state space models. In *Proceedings of the AAAI Conference on Artificial Intelligence*, volume 31, 2017.
- Rahul G Krishnan, Uri Shalit, and David Sontag. Deep kalman filters. *arXiv preprint arXiv:1511.05121*, 2015.
- Longyuan Li, Junchi Yan, Xiaokang Yang, and Yaohui Jin. Learning interpretable deep state space model for probabilistic time series forecasting. *Proceedings of the Twenty-Eighth International Joint Conference on Artificial Intelligence*, 2019.
- Bryan Lim, Sercan Arik, Nicholas Loeff, and Tomas Pfister. Temporal fusion transformers for interpretable multi-horizon time series forecasting. In *International Journal of Forecasting*, 2021.
- Christos Louizos and Max Welling. Multiplicative normalizing flows for variational bayesian neural networks. In *International Conference on Machine Learning*, pages 2218–2227. PMLR, 2017.
- Christos Louizos, Karen Ullrich, and Max Welling. Bayesian compression for deep learning. *Advances in neural information processing systems*, 30, 2017.
- Peter McCullagh and John A Nelder. *Generalized linear models*. Routledge, 2019.
- Charles E McCulloch and Shayle R Searle. *Generalized, linear, and mixed models*. John Wiley & Sons, 2004.
- Douglas C Montgomery, Cheryl L Jennings, and Murat Kulahci. *Introduction to time series analysis and forecasting*. John Wiley & Sons, 2015.
- Sarah E Neville, John T Ormerod, and MP Wand. Mean field variational bayes for continuous sparse signal shrinkage: pitfalls and remedies. *Electronic Journal of Statistics*, 8(1):1113–1151, 2014.
- William B Nicholson, David S Matteson, and Jacob Bien. Varx-l: Structured regularization for large vector autoregressions with exogenous variables. *International Journal of Forecasting*, 33(3):627–651, 2017.
- Bogdan Oancea and Ștefan Cristian Ciucu. Time series forecasting using neural networks. *arXiv preprint arXiv:1401.1333*, 2014.

- Juho Piironen and Aki Vehtari. Sparsity information and regularization in the horseshoe and other shrinkage priors. *Electronic Journal of Statistics*, 11(2): 5018–5051, 2017.
- Syama Sundar Rangapuram, Matthias W Seeger, Jan Gasthaus, Lorenzo Stella, Yuyang Wang, and Tim Januschowski. Deep state space models for time series forecasting. In *Advances in Neural Information Processing Systems*, volume 31. Curran Associates, Inc., 2018.
- Danilo Rezende and Shakir Mohamed. Variational inference with normalizing flows. In *International conference on machine learning*, pages 1530–1538. PMLR, 2015.
- Danilo Jimenez Rezende, Shakir Mohamed, and Daan Wierstra. Stochastic backpropagation and approximate inference in deep generative models. In *International conference on machine learning*, pages 1278–1286. PMLR, 2014.
- David Salinas, Valentin Flunkert, Jan Gasthaus, and Tim Januschowski. Deepar: Probabilistic forecasting with autoregressive recurrent networks. *International Journal of Forecasting*, 36:1181–1191, 2020.
- Skyler Seto, Martin T Wells, and Wenyu Zhang. Halo: Learning to prune neural networks with shrinkage. In *Proceedings of the 2021 SIAM International Conference on Data Mining (SDM)*, pages 558–566. SIAM, 2021.
- Sima Siami-Namini and Akbar Siami Namin. Forecasting economics and financial time series: Arima vs. lstm. *arXiv preprint arXiv:1803.06386*, 2018.
- Yuan Xue, Denny Zhou, Nan Du, Andrew M. Dai, Zheen Xu, Kun Zhang, and Claire Cui. Deep state-space generative model for correlated time-to-event predictions. *Proceedings of the 26th ACM SIGKDD International Conference on Knowledge Discovery and Data Mining*, pages 1552–1562, 2020.

Appendix

Hyperparameter Tuning Details

This section will detail the hyperparameter selection process for DSSM-SH for both *electricity* and *traffic* datasets. For both datasets, we generate around 450,000 samples for training and 50,000 samples for validation. This is similar to amount of samples utilized in previous work [Lim et al., 2021]. For *electricity* dataset in particular, the observed data can be drastically different in scale for different series. To control scale handling, we use a weighted sampler [Salinas et al., 2020] for the training set. The weighted sampler assigns a weight to each training sample based on the average magnitude of the response. We find in implementation that using this weighted sampler improves the training performances of the models.

In terms of hyperparameter tuning for DSSM-SH, we tune 4 parameters: the dimension for the recurrent neural network ($\dim(\mathbf{h}_t)$), the dimension for the latent variables ($\dim(\mathbf{z}_t)$), number of layers for the recurrent neural network and the learning rate for the ADAM optimizer. The choices for each of the hyperparameters are given as follows:

- $\dim(\mathbf{h}_t)$: 60, 80, 100, 120
- $\dim(\mathbf{z}_t)$: 10, 20, 30, 40
- Number of layers: 1, 2, 3
- Learning rate: $1e-3$, $1e-4$

We utilize random search in order to select the optimal hyperparameters using training/validation sets. The optimal parameters found for DSSM-SH for the *electricity* dataset is $\dim(\mathbf{h}_t) = 80$, $\dim(\mathbf{z}_t) = 30$, number of layers = 2, learning rate = $1e-3$. The resulting model has a total of 296808 number of parameters. The optimal parameters found for DSSM-SH for the *traffic* dataset is $\dim(\mathbf{h}_t) = 80$, $\dim(\mathbf{z}_t) = 20$, number of layers = 2, learning rate = $1e-3$. The resulting model has a total of 288668 number of parameters. The choices for the other hyperparameters are as follows: $\tau_0 = 1$, $c_a = 2$, $c_b = 1$. As seen, the model contains a high number of parameters, supporting the idea that adding shrinkage can be potentially very useful.

Variational Inference Details

In this section, we will give more details concerning the estimation of the cost function seen by Equation 2. Given the details about the generative and the inference portion of the models seen in Subsections 3.2 and 3.3, we start with the ELBO as follows:

$$\begin{aligned} L(\boldsymbol{\theta}, \boldsymbol{\phi}) &\equiv E_{q_{\boldsymbol{\phi}}(\mathbf{z}_{1:T}, \mathbf{h}_{1:T}, \boldsymbol{\tau}, c, \boldsymbol{\lambda}_{1:T} | \mathbf{y}_{1:T}, \mathbf{u}_{1:T})} [\log p_{\boldsymbol{\theta}}(\mathbf{y}_{1:T} | \mathbf{z}_{1:T}, \mathbf{h}_{1:T}, \boldsymbol{\tau}, c, \boldsymbol{\lambda}_{1:T}, \mathbf{u}_{1:T})] - \\ &\quad \text{KL}(q_{\boldsymbol{\phi}}(\mathbf{z}_{1:T}, \mathbf{h}_{1:T}, \boldsymbol{\tau}, c, \boldsymbol{\lambda}_{1:T} | \mathbf{y}_{1:T}, \mathbf{u}_{1:T}) || p_{\boldsymbol{\theta}}(\mathbf{z}_{1:T}, \mathbf{h}_{1:T}, \boldsymbol{\tau}, c, \boldsymbol{\lambda}_{1:T} | \mathbf{y}_{1:T}, \mathbf{u}_{1:T})) \\ &\equiv L_E - L_{KL} \end{aligned}$$

This loss has two terms which we will discuss individually. For clarity and ease of notation, we will denote the first term as L_E and the second term as L_{KL} . We will start with a discussion for the KL term followed by discussion of the expectation term. We first perform the following factorization for L_{KL} :

$$\begin{aligned} L_{KL} &= \sum_{t=1}^T E_{q_{\boldsymbol{\phi}}(\boldsymbol{\tau}, c, \boldsymbol{\lambda}_t | \mathbf{y}_t, \mathbf{h}_t, \mathbf{u}_t)} [\text{KL}(q_{\boldsymbol{\phi}}(\mathbf{z}_t | \mathbf{z}_{t-1}, \boldsymbol{\tau}, c, \boldsymbol{\lambda}_t, \mathbf{y}_t, \mathbf{h}_t, \mathbf{u}_{1:T}) || p_{\boldsymbol{\theta}}(\mathbf{z}_t | \mathbf{z}_{t-1}, \boldsymbol{\tau}, c, \boldsymbol{\lambda}_t, \mathbf{y}_t, \mathbf{h}_t, \mathbf{u}_t))] + \\ &\quad \text{KL}(q_{\boldsymbol{\phi}}(\boldsymbol{\tau}, c, \boldsymbol{\lambda}_t | \mathbf{z}_{t-1}, \mathbf{y}_{1:T}, \mathbf{u}_t, \mathbf{h}_t) || p_{\boldsymbol{\theta}}(\boldsymbol{\tau}, c, \boldsymbol{\lambda}_t)) \end{aligned}$$

This factorization allow KL-divergence terms to be written as sum of individual KL-terms across time. The reason this factorization works is due to the structure we chose for the generative and inference models shown in Figure 1. Note that $\mathbf{h}_{1:T}$ is deterministic and uses the same RNN for both the generative and inference portions. This choice leads to a KL-divergence of 0 for $\mathbf{h}_{1:T}$ which simplify the derivation.

We will now break down each term in L_{KL} . First, in the generative model, the distributions $(\boldsymbol{\tau}, c, \boldsymbol{\lambda}_t)$ do not conditional on any other variables and are independent of one another. This allow us to drop the conditional for this term. In the inference model, conditional on $(\mathbf{z}_{t-1}, \mathbf{y}_{1:T}, \mathbf{u}_t, \mathbf{h}_t)$, the approximate posterior of $(\boldsymbol{\tau}, c, \boldsymbol{\lambda}_t)$ are

independent of one another. This allow us to fully factorize $KL(q_\phi(\tau, c, \boldsymbol{\lambda}_t | \mathbf{z}_{t-1}, \mathbf{y}_{1:T}, \mathbf{u}_t, \mathbf{h}_t) || p_\theta(\tau, c, \boldsymbol{\lambda}_t))$ into separate terms and evaluated analytically. From the posterior choices seen in Equations 14 and 15 and prior choices seen in Equations 6, 7 and 9, this KL term has a closed form solution. This closed form solution relies the closed form KL-divergence formula between log-normal random variables and Gamma/inverse-Gamma random variables derived in Louizos et al. [2017].

Second, conditional on $(\mathbf{z}_{t-1}, \tau, c, \boldsymbol{\lambda}_t, \mathbf{y}_t, \mathbf{h}_t, \mathbf{u}_{1:T})$, the distribution of \mathbf{z}_t is normal for both the generative and inference portion of the model. The conditional can be written as follows:

$$\begin{aligned} q_\phi(\mathbf{z}_t | \mathbf{z}_{t-1}, \tau, c, \boldsymbol{\lambda}_t, \mathbf{y}_t, \mathbf{h}_t, \mathbf{u}_t) &\sim N(\boldsymbol{\mu}_{\phi, \mathbf{z}}(\mathbf{z}_{t-1}, \mathbf{y}_t, \mathbf{h}_t) \boldsymbol{\tau}_t^* \boldsymbol{\lambda}_t, \boldsymbol{\sigma}_{\phi, \mathbf{z}}(\mathbf{z}_{t-1}, \mathbf{y}_t, \mathbf{h}_t) \boldsymbol{\tau}_t^* \boldsymbol{\lambda}_t) \\ p_\theta(\mathbf{z}_t | \mathbf{z}_{t-1}, \tau, c, \boldsymbol{\lambda}_t, \mathbf{y}_t, \mathbf{h}_t, \mathbf{u}_t) &\sim N(\boldsymbol{\mu}_{\theta, \mathbf{z}}(\mathbf{z}_{t-1}, \mathbf{y}_t, \mathbf{h}_t) \boldsymbol{\tau}_t^* \boldsymbol{\lambda}_t, \boldsymbol{\sigma}_{\theta, \mathbf{z}}(\mathbf{z}_{t-1}, \mathbf{y}_t, \mathbf{h}_t) \boldsymbol{\tau}_t^* \boldsymbol{\lambda}_t) \end{aligned}$$

Suppose $\mathbf{z}_t \in R^Q$ where $\mathbf{z}_t = (z_{t,1}, \dots, z_{t,Q})$, the KL-divergence between the two terms can be calculated as follows:

$$\begin{aligned} &KL(q_\phi(\mathbf{z}_t | \mathbf{z}_{t-1}, \tau, c, \boldsymbol{\lambda}_t, \mathbf{y}_t, \mathbf{h}_t, \mathbf{u}_t) || p_\theta(\mathbf{z}_t | \mathbf{z}_{t-1}, \tau, c, \boldsymbol{\lambda}_t, \mathbf{y}_t, \mathbf{h}_t, \mathbf{u}_t)) \\ &= \sum_{i=1}^Q \log \frac{\sigma_{\theta, z, i}(\mathbf{z}_{t-1}, \mathbf{y}_t, \mathbf{h}_t) \tau_{t, i}^* \lambda_{t, i}}{\sigma_{\phi, z, i}(\mathbf{z}_{t-1}, \mathbf{y}_t, \mathbf{h}_t) \tau_{t, i}^* \lambda_{t, i}} \\ &\quad + \frac{\sigma_{\phi, z, i}^2(\mathbf{z}_{t-1}, \mathbf{y}_t, \mathbf{h}_t) \tau_{t, i}^{2*} \lambda_{t, i}^2 + (\mu_{\phi, z, i}(\mathbf{z}_{t-1}, \mathbf{y}_t, \mathbf{h}_t) \tau_{t, i}^* \lambda_{t, i} - \mu_{\theta, z, i}(\mathbf{z}_{t-1}, \mathbf{y}_t, \mathbf{h}_t) \tau_{t, i}^* \lambda_{t, i})^2}{2\sigma_{\theta, z, i}^2(\mathbf{z}_{t-1}, \mathbf{y}_t, \mathbf{h}_t) \tau_{t, i}^{2*} \lambda_{t, i}^2} - \frac{1}{2} \\ &= \sum_{i=1}^Q \log \frac{\sigma_{\theta, z, i}(\mathbf{z}_{t-1}, \mathbf{y}_t, \mathbf{h}_t)}{\sigma_{\phi, z, i}(\mathbf{z}_{t-1}, \mathbf{y}_t, \mathbf{h}_t)} + \frac{\sigma_{\phi, z, i}^2(\mathbf{z}_{t-1}, \mathbf{y}_t, \mathbf{h}_t) + (\mu_{\phi, z, i}(\mathbf{z}_{t-1}, \mathbf{y}_t, \mathbf{h}_t) - \mu_{\theta, z, i}(\mathbf{z}_{t-1}, \mathbf{y}_t, \mathbf{h}_t))^2}{2\sigma_{\theta, z, i}^2(\mathbf{z}_{t-1}, \mathbf{y}_t, \mathbf{h}_t)} - \frac{1}{2} \end{aligned}$$

As seen, all terms involving the shrinkage variables $(\tau, c, \boldsymbol{\lambda}_{1:T})$ cancels out in the KL-divergence. As a result,

$$\begin{aligned} &E_{q_\phi(\tau, c, \boldsymbol{\lambda}_t | \mathbf{y}_t, \mathbf{h}_t, \mathbf{u}_t)} [KL(q_\phi(\mathbf{z}_t | \mathbf{z}_{t-1}, \tau, c, \boldsymbol{\lambda}_t, \mathbf{y}_t, \mathbf{h}_t, \mathbf{u}_{1:T}) || p_\theta(\mathbf{z}_t | \mathbf{z}_{t-1}, \tau, c, \boldsymbol{\lambda}_t, \mathbf{y}_t, \mathbf{h}_t, \mathbf{u}_t))] \\ &= KL(q_\phi(\mathbf{z}_t | \mathbf{z}_{t-1}, \tau, c, \boldsymbol{\lambda}_t, \mathbf{y}_t, \mathbf{h}_t, \mathbf{u}_{1:T}) || p_\theta(\mathbf{z}_t | \mathbf{z}_{t-1}, \tau, c, \boldsymbol{\lambda}_t, \mathbf{y}_t, \mathbf{h}_t, \mathbf{u}_t)) \end{aligned}$$

This once again allows for a closed-form solution which allows for effective evaluation of the KL-divergence. This solution is one of the key reasons behind many of the design choices for the generative/inference portions of the model. By choosing approximate conditional dependencies among variables, we allow for a closed-form solution for the KL-divergence in the loss. A closed-form solution leads to more accurate gradients and faster evaluations.

Given a closed form solution for L_{KL} , we will now focus our attention to the first part of the loss: L_E . Similar to the first step in factorizing L_{KL} , we adopt the following factorization for L_E :

$$\begin{aligned} L_E &= E_{q_\phi(\mathbf{z}_{1:T}, \mathbf{h}_{1:T}, \tau, c, \boldsymbol{\lambda}_{1:T} | \mathbf{y}_{1:T}, \mathbf{u}_{1:T})} [\log p_\theta(\mathbf{y}_{1:T} | \mathbf{z}_{1:T}, \mathbf{h}_{1:T}, \tau, c, \boldsymbol{\lambda}_{1:T}, \mathbf{u}_{1:T})] \\ &= \sum_{t=1}^T E_{q_\phi(\mathbf{z}_t | \mathbf{z}_{t-1}, \mathbf{h}_t, \tau, c, \boldsymbol{\lambda}_t, \mathbf{y}_t, \mathbf{u}_t)} [\log p_\theta(\mathbf{y}_t | \mathbf{z}_t)] \end{aligned}$$

This factorization results directly from the choices we made in the generative model. Conditional on \mathbf{z}_t , the generative distribution for \mathbf{y}_t is independent of over other variables in the model as seen in Equation 10. To evaluate this expectation, we obtain samples from the approximate posterior $q_\phi(\mathbf{z}_t | \mathbf{z}_{t-1}, \mathbf{h}_t, \tau, c, \boldsymbol{\lambda}_t, \mathbf{y}_t, \mathbf{u}_t)$ and evaluate the log predictive likelihood.

Through our choices for the generative and inference portions of the model, we are able to obtain a time-based factorization of the loss. This allows the loss function to be calculated one-step at a time during training. With the closed-form KL-divergence terms, we do not need to sample any variables from the generative model in the training phase. We only need to sample from $q_\phi(\mathbf{z}_t | \mathbf{z}_{t-1}, \mathbf{h}_t, \tau, c, \boldsymbol{\lambda}_t, \mathbf{y}_t, \mathbf{u}_t)$ at each time-step t of the training process. For sampling, we utilize reparameterization trick as detailed in Section 3.4.